Electron *g*-factor anisotropy in symmetric (110)-oriented GaAs quantum wells

J. Hübner,[1,*] S. Kunz,[1] S. Oertel,[1] D. Schuh,[2] M. Pochwała,[3] H. T. Duc,[3] J. Förstner,[3] T. Meier,[3] and M. Oestreich[1]

[1]*Institute for Solid State Physics, Leibniz Universität Hannover, Appelstrasse 2, DE-30167 Hannover, Germany*
[2]*Institute for Experimental and Applied Physics, Universität Regensburg, DE-93040 Regensburg, Germany*
[3]*Department of Physics and CeOPP, Universität Paderborn, Warburger Str. 100, DE-33098 Paderborn, Germany*

We demonstrate by spin quantum beat spectroscopy that in undoped symmetric (110)-oriented GaAs/AlGaAs single quantum wells, even a symmetric spatial envelope wave function gives rise to an asymmetric in-plane electron Landé *g*-factor. The anisotropy is neither a direct consequence of the asymmetric in-plane Dresselhaus splitting nor a direct consequence of the asymmetric Zeeman splitting of the hole bands, but rather it is a pure higher-order effect that exists as well for diamond-type lattices. The measurements for various well widths are very well described within 14×14 band $\mathbf{k} \cdot \mathbf{p}$ theory and illustrate that the electron spin is an excellent meter variable for mapping out the internal—otherwise hidden—symmetries in two-dimensional systems. Fourth-order perturbation theory yields an analytical expression for the strength of the *g*-factor anisotropy, providing a qualitative understanding of the observed effects.

Symmetry is a fundamental principle which runs through all sciences like a common thread, and the balance of proportions has been attracting great interest ever since. The classification of nearly all entities in today's physics in terms of their symmetry properties is a very powerful and widely applied method in a vast number of fields. Among the plethora of interesting physical observables, the pure quantum-mechanical entity *spin* in connection with the relativistic effect of spin-orbit interaction (SOI)[1] bears an exceedingly strong connection to symmetry. In a free atom, SOI can break the degeneracy of states with the same orbital wave function owing opposite spins. In solids, however, such a splitting interferes with crystal symmetry. The most prominent example is the conduction band Dresselhaus splitting in a zinc-blende (ZB) type lattice semiconductor,[2] which is not present in its diamond lattice type equivalents.[3] The alteration of the symmetry allows a clear assignment of the investigated spin properties to the symmetry at hand and the change of symmetry properties on micro- and macroscopic scales is easy to produce in solid-state physics by the introduction of low-dimensional structures, potential gradients, or the choice of peculiar crystallographic quantization axes. This fact has boosted a great interest in recent semiconductor spintronic research[4–6] since crystal symmetry yields a control on the spin dynamics,[7–12] and contrariwise the entity *spin* yields, jointly with the time-reversal breaking property of a magnetic field, a well-suited meter variable for probing internal symmetries which might be inaccessible by other means.

In this Rapid Communication, we exploit the intriguing property that quantum wells (QWs) grown with their quantization axis along the low-symmetry [110] direction belong to the same symmetry class C_{2v} as asymmetric (001)-oriented QWs. However, the spatial part of the wave function remains symmetric in growth direction for the (110)-oriented structure and it is only the spin-dependent part, i.e., the Dresselhaus and Zeeman contributions which senses the symmetry reduction. For the (001)-oriented bulk GaAs crystals, the introduction of a two-dimensional confinement changes the primary ZB symmetry from T_d to D_{2d}. This gives rise to the anisotropy of in- and out-of-plane *g*-factors.[13–16] Further suppression of

symmetry operations—leaving only the identity operation, a two-fold rotation axis, and two mirror planes—yields C_{2v} symmetry. However, the arrangement of the mirror planes can be achieved in two different ways for ZB-based QWs: (a) by a gradient along a (001)-quantization direction which constrains all mirror planes to contain the quantization axis or (b) by the choice of the [110] axis as growth and quantization direction which places one mirror plane in the middle of the QW. The key difference between those two cases is, that in case (a) the electron spin acquires an additional dynamic due the asymmetric envelope wave function in conjunction with SOI,[11,17] whereas in case (b) the envelope wave function is fully symmetric for the electrons at the conduction band minimum. Nevertheless, the spin still acquires an additional dynamic and the in-plane *g*-factor is anisotropic also for (110)-oriented QWs.

The effective *g*-factor tensor $\hat{g}^*$ in bulk GaAs is isotropic at the Γ point but becomes increasingly anisotropic with the reduction of symmetry by heterostructure growth, potential gradients, or low symmetry growth axis. The *g*-factor tensor reduces for asymmetric (001) and symmetric (110) GaAs QWs to

$$\hat{g}^*_{C_{2v}^{001}} = \begin{pmatrix} g_s & g_a & 0 \\ g_a & g_s & 0 \\ 0 & 0 & g_z \end{pmatrix}, \quad \hat{g}^*_{C_{2v}^{110}} = \begin{pmatrix} g_s & 0 & 0 \\ 0 & g_s + 2g_a & 0 \\ 0 & 0 & g_z \end{pmatrix}, \quad (1)$$

where g_s is the in-plane *g*-factor, g_a the in-plane *g*-factor anisotropy, and g_z the *g*-factor in the growth direction. The *in-plane g*-factor anisotropy based upon asymmetric (001)-oriented structures has been examined in detail in the past[11,18,19] and a vast number of works exist on *in and out-of-plane g*-factor anisotropy. However, symmetric, GaAs-based (110)-oriented QWs have drawn a tremendous amount of attention in the past due to vanishing Dresselhaus splitting for spins aligned along the growth direction,[20–24] and the *g*-factor tensor is defined according to Eq. (1) for C_{2v}^{110} symmetry,[25] i.e., C_{2v}^{110} symmetry requires that only three independent diagonal entries of the *g*-factor tensor are nonzero.

In the following, we present detailed experimental measurements on the in-plane *g*-factor anisotropy in (110)-oriented QWs in dependence of the QW width and show that the

high-accuracy experiments are in excellent agreement with sophisticated 14×14 $\mathbf{k} \cdot \mathbf{p}$ calculations. The investigated sample is grown by molecular beam epitaxy and consists of ten undoped, symmetrical, (110)-oriented, GaAs/Al$_{0.32}$Ga$_{0.68}$As single QWs with thicknesses of 3, 4, 5, 6, 7, 8, 10, 12, 15, and 19 nm, separated by 80-nm barriers. With decreasing well width, the electronic wave function is affected stronger by the two-dimensional nature of the confining potential. However, in the limit of a vanishing well width, the wave function regains its three-dimensional nature again. From experiments measuring the exciton binding energy[26] this is expected to happen at a well width of about 4 nm for the given system.

Information about the g-factor in GaAs QWs can be reliably accessed by measuring the polarization resolved time evolution of the photoluminescence (PL) of an optically excited spin polarization with a perpendicular magnetic field applied. This technique is known as spin quantum beat spectroscopy;[27] the sample is mounted in Voigt geometry on a rotating sample holder with the growth and excitation axis perpendicular to the magnetic field axis in a helium flow cryostat with optical access within a split coil superconducting magnet. Spin polarized carriers are excited by circularly polarized laser pulses from an 80-MHz picosecond Ti:sapphire laser, and the PL is detected in the backward direction and energy- and time-resolved by a spectrometer and a synchroscan streak camera. A switchable retardation plate and a polarizer perform the polarization resolution. Spin quantum beats occur due to the time evolution of the coherently excited Zeeman-split levels of spin-up and spin-down conduction band states. The beat (Larmor) frequency ω_L is directly linked to the electron g-factor g^* and the magnetic field strength B by $\hbar\omega_L = g^* \mu_B B$. The hole spin dynamic is insignificant in the investigated experimental regime due to the fast hole spin relaxation times.

The measured effective g-factor g^* is extracted from the polarization resolved intensity modulation for different orientations of the in-plane magnetic field. Figure 1 shows the dependence of g^* on the angle between the [1$\bar{1}$0] axis and the
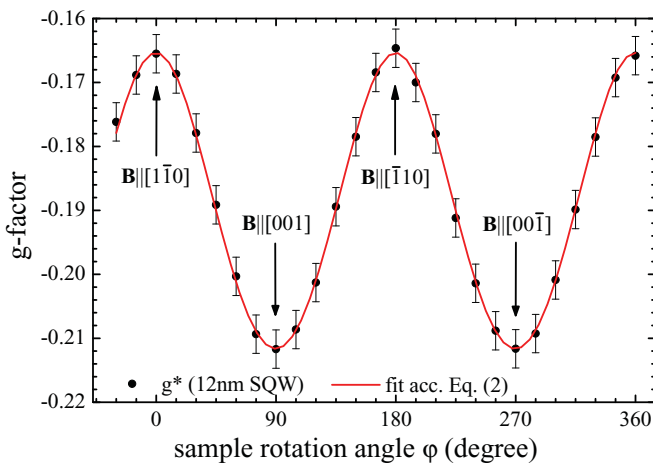
in-plane magnetic field $\mathbf{B} = B_0(\sin\varphi, \cos\varphi, 0)$. The values for the symmetric (g_s) and antisymmetric (g_a) contribution to g^* are extracted according to the equation

$$
\begin{aligned}
g^*_{\text{meas}} &= \pm \left| \hat{g}^*_{C_{2v}^{110}} \cdot \mathbf{B} \right| \Big/ B_0 \\
&= \pm \sqrt{g_s^2 + 2(g_s + g_a)g_a[1 + \cos(2\varphi + \phi_0)]}.
\end{aligned}
\tag{2}
$$

The free parameter ϕ_0 adjusts for the alignment mismatch of the sample with respect to the magnetic field axis.

Figure 2 shows the measured g-factors (squares) for all ten QW widths measured simultaneously within the same sample in dependence on the angle φ. The measurement proves a significant in-plane g-factor anisotropy and shows a continuous increase of g^* with decreasing QW width. With decreasing well width, (a) the Larmor precession frequency passes a minimum at a well width of about 7 nm, (b) the lifetime of the detected PL decreases due to higher electron-hole overlap, and (c) the spectra are more inhomogeneously broadened due to growth imperfections. The inhomogeneous broadening affects the quality of the polarization resolved spin
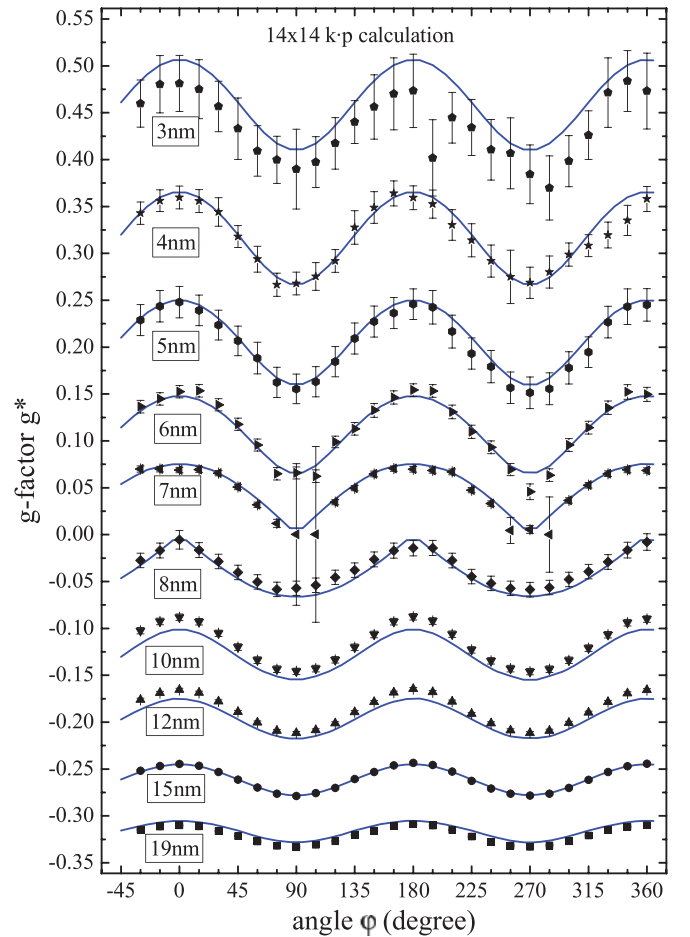

FIG. 1. (Color online) Measured electron g-factor for the 12-nm, (110)-oriented, GaAs/Al$_{0.32}$Ga$_{0.68}$As, single QW in dependence on the angle φ between the [1$\bar{1}$0] in-plane axis and the in-plane magnetic field orientation ($B = 6$ T, $T = 20$ K).[25] The line is a fit to the data according to Eq. (2) with $g_s = -0.212$, $g_a = +0.023$, and $\phi = 6.96$ mrad.

FIG. 2. (Color online) Measured g-factors (squares) in dependence on the angle φ for all ten QWs. The applied magnetic field is 6 T and the sample temperature 20 K. Note that the depicted values and curves are not shifted and all values correspond to the left axis. Calculations are with a 14×14 $\mathbf{k} \cdot \mathbf{p}$ model and a single common parameter set (solid lines).
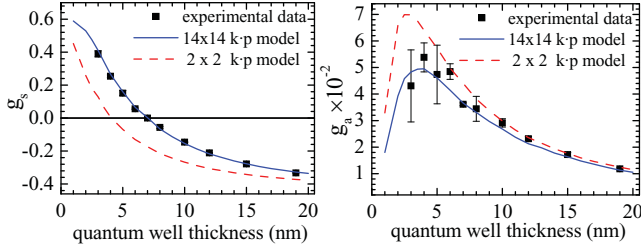
FIG. 3. (Color online) The fitting values of g_s (left) and g_a (right) as a function of well width (squares). Calculations by a 14×14 Hamiltonian (solid lines), by a simplified 2×2 Hamiltonian using fourth-order Löwdin perturbation theory (dashed lines).

quantum beats and thus increases the error of the extracted g-factor. The values for g_s and g_a with decreasing QW width are extracted according to Eq. (2) and depicted in Fig. 3. The sign of the measured g-factor depends on the energy dependence of g^* (Refs. 28–30) and on the penetration of the wave function into the barrier material which has a positive g-factor. As a consequence g_s increases monotonically with decreasing well width, i.e., increasing confinement energy. On the other hand g_a reaches a maximum at a QW width of about 4 nm where the electronic wave function is most strongly localized in the quantization direction.

In the next section, we develop a theoretical description of the observed results based upon **k·p** perturbation theory. We follow the treatment of the 14-band extended Kane model[31,32] in which the spin-orbit interaction is included to calculate the dispersions and Zeeman splitting. Input parameters are the critical point energies, the interband matrix elements (P, P', Q), and k-linear terms due to SOI (C_k). The contributions from remote bands are computed via the parameters $m^*, \gamma_{1,2,3}, g^*, \kappa$, and q as described in Refs. 31 and 32. Magnetic interaction in the presence of an in-plane magnetic field $\mathbf{B} = (B_x, B_y, 0)$ is taken into account by transformation of the quasi-momentum into the canonical momentum $\hat{k}_x = k_x + \frac{e}{\hbar} z B_y$ and $\hat{k}_y = k_y - \frac{e}{\hbar} z B_x$. We use the envelope function approximation for QW systems described by the effective-mass equation

$$\sum_{i=1}^{14} \left[H_{i,j}(\hat{\mathbf{k}}) + V_i(z)\delta_{i,j} + H_{i,j}^Z \right] \psi_{i,\mathbf{k}_\parallel}(z) = E\psi_{j,\mathbf{k}_\parallel}(z), \quad (3)$$

where H is the **k·p** Hamiltonian with $\hat{k}_z$ being replaced by the momentum operator $\hat{k}_z = -i\partial/\partial z$, $\mathbf{k}_\parallel$ is the in-plane wave vector, $V(z)$ is the band offset potential, and H^Z

is an effective Zeeman Hamiltonian including remote-band contributions. Euler rotations of the coordinate system are applied to obtain the 14×14 **k·p** Hamiltonian matrix for various crystallographic directions for the quantization axis (z axis).[10] We solve Eq. (3) by expanding the envelope functions via a plane-wave basis.[33,34] From the obtained band structure we compute the spin splitting between two spin states of the lowest conduction band $\Delta E_{k_\parallel} = E_{k_\parallel}^{(+)} - E_{k_\parallel}^{(-)}$. This splitting includes, for materials with bulk inversion asymmetry like GaAs, both Dresselhaus and Zeeman splitting. At the band edge ($k_\parallel = 0$), the Dresselhaus term vanishes and $\Delta E_{k_\parallel=0}$ is a pure Zeeman splitting. The electron g-factor is extracted from the Zeeman splitting as $g^* = \Delta E_{k_\parallel=0}/\mu_B B$.

Figure 2 shows the calculated (solid lines) electron g-factor for all ten QWs as a function of the angle between magnetic field direction and [$1\bar{1}0$] axis. The calculation is based on the full 14×14 Hamiltonian using the band parameters listed in Table I. The comparison shows an excellent agreement between theory and experiment.

Next, we carry out further analyses to understand the origin of the g-factor anisotropy within **k·p** theory. We use the Löwdin perturbation method[32] to block-diagonalize the 14×14 Hamiltonian and obtain a simplified 2×2 Hamiltonian describing the conduction band states. The terms $\hat{k}_z^n$ and z^n are replaced by the expectation values $\langle \hat{k}_z^n \rangle$ and $\langle z^n \rangle$ of the quasi-two-dimensional system. The expectation values with odd n vanish in symmetric QWs, e.g., $\langle \hat{k}_z \rangle = 0$, $\langle z \rangle = 0$. Up to fourth order of perturbation, the Hamiltonian for an electron in a QW is written as $H = H^{m^*} + H^{\text{BIA}} + H^B$. The first term H^{m^*} describes the parabolic dispersion with effective mass m^*. The second term H^{BIA} describes the Dresselhaus spin splitting due to the bulk inversion asymmetry. The third term H^B represents the linear dependence of the Hamiltonian on magnetic field (terms of second and higher order in B are neglected). The Hamiltonian H^B takes for $k_\parallel = 0$ and the QW growth axis $z \parallel [110]$ the form

$$H^B = \left(\frac{g^*}{2}\mu_B + \alpha\langle\hat{k}_z^2\rangle \right)(\sigma_x B_x + \sigma_y B_y) + \beta\langle\hat{k}_z^2\rangle\sigma_y B_y, \quad (4)$$

where σ_i are the Pauli matrices. The first term in Eq. (4) scaling with α (see Ref. 35) describes the isotropic, and the last term

TABLE I. Band parameters for GaAs and Al$_{0.32}$Ga$_{0.68}$As.[a] $E_g, E_g', \Delta, \Delta', \bar{\Delta}$ are in units of eV and P, P', Q, C_k in eV nm and m^* in m_0. The valence band offset is $\Delta E_v = 0.35\Delta E_g$.

	E_g	E_g'	Δ	Δ'	$\bar{\Delta}$	P	P'	Q
GaAs	1.517	4.504	0.341	0.171	-0.05	1.049	0.445	0.821
AlGaAs	2.019	4.655	0.330	0.164	-0.102	1.008	0.462	0.806
	$-C_k$	m^*	γ_1	γ_2	γ_3	g^*	κ	q
GaAs	0.00034	0.0665	6.98	2.06	2.93	-0.44	1.2	0.01
AlGaAs	0.00017	0.0927	5.95	1.66	2.45	0.60	0.54	0.01

[a]References are found in the supplemental material (see Ref. 35).

describes the anisotropic Zeeman splitting scaling with

$$\beta = \frac{e\,(3\hbar)^{-1}P^2Q^2}{E_g(E_g-E_g'-\Delta')}\left[\frac{4E_g+\Delta}{E_g(E_g+\Delta)} - \frac{4(E_g-E_g'-\Delta')}{E_g(E_g-E_g')}\right]$$
$$+ \frac{e\,(3\hbar)^{-1}P'^2Q^2}{(E_g-E_g'-\Delta')^2}\left[\frac{-3E_g+\Delta}{E_g(E_g+\Delta)} + \frac{3(E_g-E_g'-\Delta')}{(E_g-E_g')E_g}\right]. \quad (5)$$

We notice that for QWs grown with $z\|[001]$, the Hamiltonian H^B has the same isotropic term as in Eq. (4) but the anisotropic term vanishes, i.e., $\beta = 0$. Furthermore, Eq. (5) perfectly demonstrates the link between the g-factor anisotropy and SOI since in the limit of zero spin-orbit gaps, $\Delta = \Delta' = 0$, all intricate g-factor peculiarities disappear leaving only the free electron g-factor.

Diagonalizing the Hamiltonian in Eq. (4), we obtain $\Delta E^B_{\mathbf{k}_\|=0} = g^*(\varphi)\mu_B B_0$, where $g^*(\varphi)$ matches the relation for g^*_{meas} in Eq. (2) with the analytical expressions for $g_s = g^* + \frac{2}{\mu_B}\alpha\langle\hat{k}_z^2\rangle$ and $g_a = \frac{1}{\mu_B}\beta\langle\hat{k}_z^2\rangle$. The electron confined energy reduces to zero for well widths $d \rightarrow 0$ or $d \rightarrow \infty$, i.e., $\langle\hat{k}_z^2\rangle \rightarrow 0$, the anisotropic term vanishes, and the g-factor becomes isotropic again. The results obtained by the fourth-order perturbation approach are depicted in Fig. 3 and obviously higher-order terms are necessary to correctly reproduce the symmetric (g_s) and antisymmetric (g_a) g-factor for the given parameter set.

We note that for diamond lattices (point group O_h) the terms P', $\bar{\Delta}$, and C_k vanish.[32] However, (110)-grown heterostructures like Si/Ge/Si have the symmetry of the point group D_{2h} and will still exhibit an anisotropic *in-plane g* factor, as seen in the first term of Eq. (5), which is proportional to P and Q only. As a consequence, the asymmetry in symmetric (110)-grown structures can be attributed to the interaction of the valence and upper conduction band states ($\propto Q$), coupled to the lowest conduction band ($\propto P, P'$). We want to point out that theory also predicts a significant in-plane anisotropy of the effective mass of, e.g., 2.7% for the 12-nm QW. An in-plane effective mass anisotropy has already been observed for *asymmetric* (001)-grown QW structures.[36]

In conclusion we investigated the anisotropy of the electron Landé g-factor at low temperatures in symmetrically grown (110)-oriented GaAs/AlGaAs QWs via PL measurements. In contrast to asymmetric (001)-grown QWs with either a built-in potential gradient or an external applied electrical field, the symmetry reduction inherently originates from the low symmetry growth direction of the QW structure. The g factors for all QW widths are accurately modeled by 14×14 **k·p** theory and the source terms for the in-plane anisotropy are extracted by fourth-order perturbation theory.

*jhuebner@nano.uni-hannover.de

[1] L. H. Thomas, Nature (London) **117**, 514 (1926).
[2] G. Dresselhaus, Phys. Rev. **100**, 580 (1955).
[3] L. E. Golub and E. L. Ivchenko, Phys. Rev. B **69**, 115333 (2004).
[4] I. Zutic *et al.*, Rev. Mod. Phys. **76**, 323 (2004).
[5] J. Fabian *et al.*, Acta Phys. Slov. **57**, 565 (2007).
[6] M. Wu *et al.*, Phys. Rep. **493**, 61 (2010).
[7] Y. A. Bychkov and E. I. Rashba, J. Phys. C **17**, 6039 (1984).
[8] S. D. Ganichev *et al.*, Phys. Rev. Lett. **92**, 256601 (2004).
[9] S. A. Tarasenko, Phys. Rev. B **80**, 165317 (2009).
[10] H. T. Duc, J. Forstner, and T. Meier, Phys. Rev. B **82**, 115316 (2010).
[11] P. S. Eldridge, J. Hubner, S. Oertel, R. T. Harley, M. Henini, and M. Oestreich, Phys. Rev. B **83**, 041301 (2011).
[12] V. Lechner *et al.*, Phys. Rev. B **83**, 155313 (2011).
[13] E. L. Ivchenko and A. A. Kiselev, Sov. Phys. Semicond. **26**, 827 (1992).
[14] P. L. Jeune *et al.*, Semicond. Sci. Technol. **12**, 380 (1997).
[15] A. Malinowski, R. S. Britton, T. Grevatt, R. T. Harley, D. A. Ritchie, and M. Y. Simmons, Phys. Rev. B **62**, 13034 (2000).
[16] P. Pfeffer and W. Zawadzki, Phys. Rev. B **74**, 233303 (2006).
[17] V. K. Kalevich and V. L. Koronev, J. Exp. Theor. Phys. **56**, 253 (1992).
[18] M. Oestreich *et al.*, Europhys. Lett. **31**, 399 (1995).
[19] Y. A. Nefyodov *et al.*, Phys. Rev. B **83**, 041307 (2011).
[20] M. I. Dyakonov and V. Y. Kachorovskii, Sov. Phys. Semicond. **20**, 110 (1986).
[21] Y. Ohno *et al.*, Phys. Rev. Lett. **83**, 4196 (1999).
[22] G. Salis *et al.*, Phys. Rev. Lett. **86**, 2677 (2001).
[23] S. Döhrmann, D. Hagele, J. Rudolph, M. Bichler, D. Schuh, and M. Oestreich, Phys. Rev. Lett. **93**, 147405 (2004).
[24] M. M. Glazov, M. A. Semina, and E. Y. Sherman, Phys. Rev. B **81**, 115332 (2010).
[25] The transformation into the [110]-coordinate system yields $x' = [001]$, $y' = [1\bar{1}0]$, $z' = [110]$.
[26] R. L. Greene and K. Bajaj, Solid State Commun. **45**, 831 (1983).
[27] J. Hubner and M. Oestreich, in *Spin Physics in Semiconductors*, edited by M. I. Dyakonov (Springer, Berlin, 2008).
[28] E. L. Ivchenko and G. E. Pikus, *Superlattices and other Heterostructures* (Springer, Berlin, 1997).
[29] P. Pfeffer and W. Zawadzki, Phys. Rev. B **74**, 115309 (2006).
[30] W. Shichi *et al.*, Jpn. J. Appl. Phys. **48**, 063002 (2009).
[31] H. Mayer and U. Rössler, Phys. Rev. B **44**, 9048 (1991).
[32] R. Winkler, *Spin-Orbit Coupling Effects in Two-Dimensional Electron and Hole Systems* (Springer, Berlin, 2003).
[33] P. von Allmen, Phys. Rev. B **46**, 15382 (1992).
[34] M. Elkurdi, G. Fishman, S. Sauvage, and P. Boucaud, Phys. Rev. B **68**, 165333 (2003).
[35] See Supplemental Material at http://link.aps.org/supplemental/10.1103/PhysRevB.84.041301.
[36] T. Reker, M. Im, L. E. Bremme, H. Choi, Y. Chung, P. C. Klipstein, and H. Shtrikman, Phys. Rev. Lett. **88**, 056403 (2002).